

Local and regional Indian Summer Monsoon precipitation dynamics during Termination II and the Last Interglacial

Matthias Magiera¹, Franziska A. Lechleitner², Andrea M. Erhardt³, Adam Hartland⁴, Ola Kwiecien⁵, Hai Cheng^{6,7}, Harold J. Bradbury⁸, Alexandra V. Turchyn⁸, Sylvia Riechelmann⁵, Lawrence Edwards⁷, and Sebastian F.M. Breitenbach⁵

¹Department of Biological and Geographical Sciences, University of Huddersfield, UK

²Department of Earth Sciences, University of Oxford, UK

³Department of Earth and Environmental Sciences, University of Kentucky, Lexington, KY 40506, USA

⁴Environmental Research Institute, University of Waikato, Hamilton, New Zealand

⁵Institute of Geology, Mineralogy and Geophysics, Ruhr-University Bochum, 44801 Bochum, Germany

⁶Institute of Global Environmental Change, Xi'an Jiaotong University, Xi'an 710049, China

⁷Department of Earth Sciences, University of Minnesota, Minnesota 55455, USA

⁸Department of Earth Sciences, University of Cambridge, UK

Key Points:

- First multi-proxy stalagmite record from the Indian Summer Monsoon domain covering Termination II and Marine Isotope Stage 5e
- Combined use of $\delta^{18}\text{O}$, $\delta^{44}\text{Ca}$ and elemental data to discriminate between rainfall source and amount, and local infiltration
- The rainy season during Marine Isotope Stage 5e was wetter, likely with more extreme rainfall events, compared to the Holocene

Corresponding author: Matthias Magiera, Matthias.Magiera@gmail.com

Abstract

To date Indian Summer Monsoon (ISM) dynamics have been assessed by changes in stalagmite $\delta^{18}\text{O}$. However, stalagmite $\delta^{18}\text{O}$ is influenced by multiple environmental factors (e.g. atmospheric moisture transport, rainfall amount at the study site, ISM seasonality), precluding simple and clear reconstructions of rainfall amount or variability. This study aims to disentangle these environmental factors by combining $\delta^{18}\text{O}$, $\delta^{44}\text{Ca}$ and elemental data from a stalagmite covering Termination II and the last interglacial from Mawmluh Cave, NE India, to produce a semi-quantitative reconstruction of past ISM rainfall. We interpret $\delta^{18}\text{O}$ as a mixed signal of rainfall source dynamics and rainfall amount, and coupled $\delta^{44}\text{Ca}$ and X/Ca ratios as indicators of local infiltration rate and prior calcite precipitation in the karst zone. The wettest conditions in our studied interval (135 and 100 kyrs BP (BP = before present, with the present being 1950 CE)) occurred during MIS-5e. Our multi-proxy dataset suggests a likely change in seasonal distribution of MIS-5e rainfall compared to the Holocene; the wet season was longer with higher-than-modern dry season rainfall. Using the last interglacial as an analogue for future anthropogenic warming, our data suggest a more erratic ISM behavior in a warmer world.

1 Introduction

Precipitation in north-eastern India is governed by the ISM, which is part of the Asian Summer Monsoon (ASM) system, one of the largest and most studied atmospheric circulation systems on Earth [Buckley *et al.*, 2014]. With the ASM affecting 60% of Earth's population, understanding its present and past dynamics is vital for assessing future risks associated with anthropogenic climate change (e.g. flooding and/or crop failure) [Shukla *et al.*, 2011]. While Holocene and modern ISM dynamics are relatively well understood [Berkelhammer *et al.*, 2010; Ziegler *et al.*, 2010; Sinha *et al.*, 2015; Myers *et al.*, 2015; Kathayat *et al.*, 2016; Lechleitner *et al.*, 2017; Ronay *et al.*, 2019], ongoing anthropogenic global warming provides incentive to investigate past periods of even higher global temperatures. One such warm period, the last interglacial, (Marine Isotope Stage 5e – MIS-5e [Shackleton *et al.*, 2003; Railsback *et al.*, 2015]) was characterized by minor ice sheet coverage at high latitudes [Shackleton *et al.*, 2003; Yin and Berger, 2015; Jia *et al.*, 2016; Berger *et al.*, 2016], and higher-than-modern temperatures and sea level [Burns, 2002; Berkelhammer *et al.*, 2010; Siccha *et al.*, 2015], and provides a potential analogue for future climate conditions [Fischer *et al.*, 2018].

Here, we present a new multi-proxy stalagmite record from Mawmluh Cave, north-eastern India, covering the Termination II (T II: 134 - 130 kyrs BP) to late MIS-5e interval. We combine stalagmite $\delta^{44}\text{Ca}$, $\delta^{18}\text{O}$, and elemental (X/Ca) measurements with the objective to disentangle local from regional precipitation

dynamics. Due to the paucity of well-dated, high-resolution, continental records from the ISM domain covering the penultimate glacial/interglacial transition, we focus in the first instance on process-oriented interpretation of our data rather than comparison with other records.

1.1 Study site and modern climate

Mawmluh Cave is located on the Meghalaya Plateau in north-eastern India (25°15'44"N, 91°52'54"E, 1160 m above sea level; Fig. 1a). Mean annual precipitation at the site amounts to an average of ~10,000 mm per year (<http://climexp.knmi.nl>), with 75% of rainfall occurring during the ISM season (June to mid-October; Fig. 1a). During the ISM season, moisture is delivered to Mawmluh Cave principally by advection of air masses from the Bay of Bengal (BoB) branch of the ISM towards the Meghalaya Plateau. Orographic forcing of the Meghalaya Plateau leads to adiabatic cooling of the air masses and extreme rainfall during the ISM (Fig. 1a). Rainfall $\delta^{18}\text{O}$ values are lowest during the ISM season, due to a combination of four factors: i) moisture source location (Asian continent or Indian Ocean), ii) air mass travel distance from the BoB and the Indian Ocean (rainout effect), iii) temporal changes in the moisture source isotopic composition due to freshwater runoff from the Asian continent, iv) isotopic disequilibrium between seawater and vapor during stormy weather. During the pre-ISM (January to May) higher $\delta^{18}\text{O}$ values are indicative of low precipitation, due to a shorter transport pathway as moisture largely originates from the BoB. In the post-ISM months (mid-October to December), a more proximal moisture source in the BoB is combined with a freshwater effect due to increased summer runoff from the Tibetan Plateau, resulting in lower $\delta^{18}\text{O}$ values than would be expected from a proximal moisture source [Breitenbach *et al.*, 2010]. These changes are also seen in Mawmluh Cave dripwater, where pre-ISM $\delta^{18}\text{O}$ is higher than ISM and post ISM $\delta^{18}\text{O}$ (Fig. 1a) and $\delta^{18}\text{O}$ is highest when infiltration is minimal during the dry season [Breitenbach *et al.*, 2010; Breitenbach *et al.*, 2015]. Changes in the timing of the reversal of the circulation patterns (i.e. seasonality) likely have a strong effect on the length and intensity of the wet and dry seasons and thus on ISM “strength”, with a longer-lasting ISM resulting in more depleted $\delta^{18}\text{O}$.

82

83

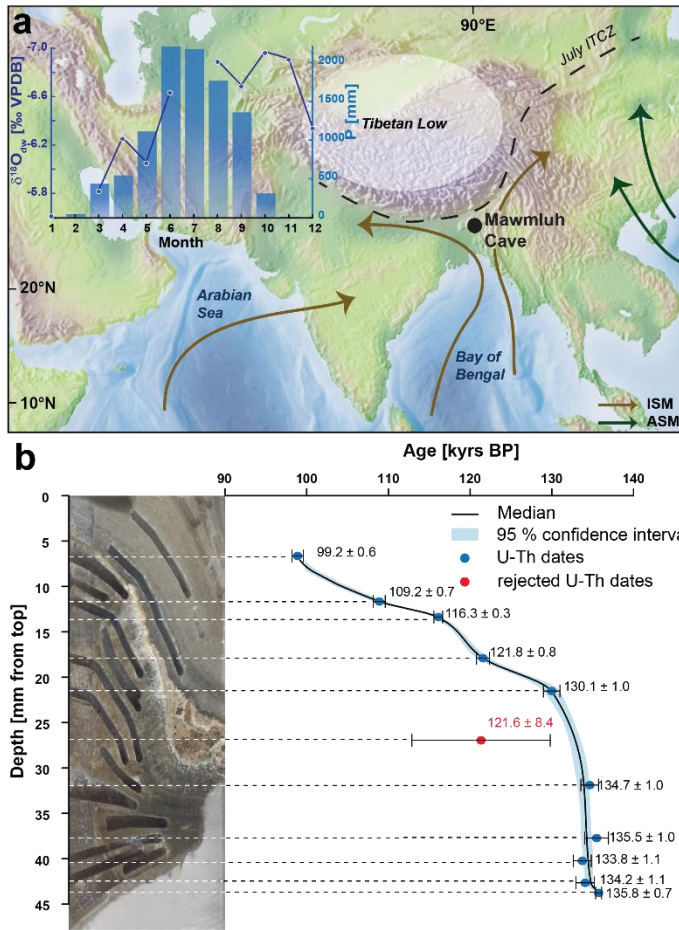


Figure 1: Location of Mawmluh Cave and the summer monsoon branches, and sample details: The prevailing wind trajectories of the ISM are denoted by brown arrows, and by green arrows for the ASM (adapted from Lechleitner et al., 2017). The climate diagram shows rainfall amount (in mm) and dripwater $\delta^{18}O$ (‰ VPDB) per month (data obtained from Breitenbach et al. 2015) (a); Subsample MAW-3_7 and age-depth model based on interpolation between the U-Th dates. Black dots denote U/Th samples with their errors, blue shading indicates the 95 % confidence interval and the black line denotes the median of the COPRA age-depth model (b).

1.2 Speleothems as precipitation archives

To date speleothems are the most robustly-dated and highest-resolved archives of ASM precipitation variability [Wang et al., 2001; Yuan et al., 2004; Johnson et al., 2006; Cai et al., 2015; Cheng et al., 2016]. Past studies focused on stalagmite $\delta^{18}O$ to explore changes in monsoon intensity, where stalagmite $\delta^{18}O$ is influenced by combined local (e.g. rainfall amount, infiltration patterns within the aquifer, and length of the rainy season) and regional factors (moisture source location and atmospheric transport of water vapor) [Dykoski et al., 2005; Baker et al., 2015; Cheng et al., 2016; Kukla et al., 2019]. In general, more negative

stalagmite $\delta^{18}\text{O}$ is interpreted as higher monsoon intensity, and more positive $\delta^{18}\text{O}$ as lower monsoon intensity [Fairchild and Baker, 2012]. However, with the multitude of factors influencing speleothem $\delta^{18}\text{O}$, reconstructing regional and local monsoon dynamics based on this proxy alone remains challenging [Gupta et al., 2005; Breitenbach et al., 2010; Pausata et al., 2011; Dreybrodt and Scholz, 2011; Lechleitner et al., 2017].

The key to disentangling local from regional effects in past precipitation patterns lies in the aquifer above the cave. Rainwater leaches Ca from soil and bedrock and transports it to the cave through the karst. Upon reaching the cave, the lower cave atmosphere pCO_2 causes the carbonate and Ca-enriched fluid to degas, resulting in carbonate precipitation. Carbonate precipitation might also occur within the karst zone, e.g. in air-filled pockets, a process termed prior carbonate precipitation (PCP) [Fairchild and Baker, 2012]. Infiltration amount is one major factor controlling PCP: infiltration increases during heavy rainfall, filling pores and voids within the aquifer with water which in turn increases the velocity of water moving through the karst zone and decreases the residence time of the solution in the aquifer. Together, these processes combine to minimize PCP, while reduced infiltration conversely enhances PCP, thus linking PCP to local rainfall amount [Sherwin and Baldini, 2011; Owen et al., 2016]. Apart from infiltration amount, the length of the pathway the water has to cover to reach the cave is a second factor controlling PCP. A longer pathway, with increased water residence time within the karst zone will result in increased PCP. However, when considering variability in PCP over time, the influence of pathway length is likely of secondary importance compared to infiltration amount, and thus using PCP as measure for infiltration amount is justified [Tadros et al., 2016].

Elemental ratios (X/Ca ; here Mg/Ca , Sr/Ca , Ba/Ca) measured in speleothems are the most widely applied proxy for PCP [Fairchild and Baker, 2012]. Given the similar size and ionic radii of Mg^{2+} , Sr^{2+} , and Ba^{2+} , the incorporation of these elements into calcite occurs via substitution of Ca^{2+} [McIntire, 1963; Fairchild and Baker, 2012]. When PCP occurs in the karst, Ca is incorporated into calcite while incompatible elements stay in solution where their ratio to Ca (X/Ca) increases; this is reflected in increased speleothem X/Ca values.

Since the partitioning of Mg/Ca, Sr/Ca, and Ba/Ca are also influenced by temperature and fluid elemental composition [Fairchild and Baker, 2012; Day and Henderson, 2013], X/Ca values provide important but not yet quantitative information on past karst hydrological changes [Huang and Fairchild, 2001; Owen et al., 2016]. Calcium isotope ratios (measured as $\delta^{44/40}\text{Ca}$, referred hereafter as $\delta^{44}\text{Ca}$) have recently emerged as a promising new proxy for PCP [Reynard et al., 2011; Owen et al., 2016]. The $\delta^{44}\text{Ca}$ of calcite is influenced by the calcite growth rate, which is controlled by the rate of CO_2 degassing and the saturation state of the solution with respect to calcium carbonate. During carbonate mineral precipitation, light ^{40}Ca isotopes are preferentially incorporated into the precipitate due to kinetic isotope fractionation [Reynard et al., 2011; Yan et al., 2016; Owen et al., 2016; Li et al., 2018], leaving the fluid enriched in ^{44}Ca . Thus, increased infiltration and minimal PCP during wet periods is expected to result in lower stalagmite $\delta^{44}\text{Ca}$ values, while periods of reduced infiltration and enhanced PCP will be reflected in increased stalagmite $\delta^{44}\text{Ca}$ [Owen et al., 2016].

2 Materials and methods

The 125 cm long stalagmite MAW-3 was collected from Mawmluh Cave in 2007. To evaluate modern seasonal variability in $\delta^{44}\text{Ca}$ values and calculate a site-specific fractionation factor we used two modern carbonate precipitates, MAW-Mod-1 (collected from a glass plate in 2007) and MAW-logger (formed on a drip logger in 2013), and compared them to nine dripwater (5 pre-ISM, 2 ISM, and 2 post-ISM) and two host rock samples, collected in 2007 and 2013 (Table S3 in supplementary information, SI). The mineralogy of MAW-3_7 and the two modern precipitates was determined using X-ray diffraction (XRD) on a Panalytical Empyrean powder diffractometer (PANalytical B.V., Almelo, The Netherlands) at RUB. We focus here on the lowermost 7 cm of the sample section MAW-3_7 (Fig. 1b). The chronology of MAW-3_7 is constrained by 10 U-Th dates (Fig. 1b) (Table S2), analyzed by multicollector inductively coupled mass spectrometry (MC-ICP-MS) using a Thermo-Finnigan Neptune in the Minnesota Isotope Laboratory following the methodology of [Edwards et al., 1987; Cheng et al., 2013]. The age model was

constructed by applying a cubic interpolation procedure using COPRA [Breitenbach *et al.*, 2012].

A total of 108 samples (Table S1 in SI) were milled at a spatial resolution of 0.4 mm along the stalagmite growth axis using a CAM 100 (vhf) micro-mill at Ruhr-University Bochum (RUB). An aliquot of 87 samples were analyzed for $\delta^{18}\text{O}$ and $\delta^{13}\text{C}$ on a ThermoFisher Scientific MAT 235 IRMS equipped with a GasBench II at RUB, following the procedure of [Breitenbach and Bernasconi, 2011]. Based on an in-house carbonate standard the 1σ reproducibility is $\pm 0.07\text{‰}$ for $\delta^{18}\text{O}$ (2015-2016). All values are reported in ‰ relative to the Vienne Pee-Dee Belemnite (VPDB) standard. Aliquots from 25 samples were analyzed for elemental ratios using a Perkin-Elmer Elan quadrupole ICP-MS at the University of Waikato, however only 13 out of 25 samples have yielded results due to insufficient sample material. The samples were standardized using a NIST-certified external standard solution (see SI for details). Aliquots of 33 stalagmite samples, the dripwater samples, the modern calcite sample MAW-logger and two host rock samples were analyzed for $\delta^{44}\text{Ca}$ ($\delta^{44/40}\text{Ca}$) on a ThermoFisher Scientific Triton Plus Thermal Ionisation Mass Spectrometer in the Department of Earth Sciences at the University of Cambridge, following the method of [Bradbury and Turchyn, 2018]. The average external 2σ standard deviation over 9 months on the standard NIST 915B was 0.1‰ (mean = -0.28 , $n = 82$) (Text S1 in SI).

The modern aragonite precipitate of MAW-Mod-1 was analysed for $\delta^{44/42}\text{Ca}$ on a ThermoFisher Scientific Neptune MC-ICP-MS at RUB. The long-term reproducibility of the standard SRM-915a is $\delta^{44/42}\text{Ca}_{\text{IAPSO}} = -0.99 \pm 0.09 \text{‰}$ (2σ), ($\delta^{44/42}\text{Ca}_{\text{BSE}} = -1.13 \pm 0.19 \text{‰}$ (2σ); $n = 79$; January to September 2017), which is in agreement with previously published values [Steuber and Buhl, 2006; Hippler *et al.*, 2013; Gussone *et al.*, 2016a]. All calcium isotope data are reported relative to Bulk Silicate Earth (BSE) reference standard.

For a comparison with the Ca isotope values obtained at Cambridge, the $\delta^{44/42}\text{Ca}$ values measured at RUB are converted to $\delta^{44}\text{Ca}$ using the following equation [Harouaka *et al.*, 2016]:

$$\delta^{44}\text{Ca} = \delta^{44/42}\text{Ca} * \frac{41.9586}{39.9626} * \frac{39.9626 - 43.9555}{41.9586 - 43.9555} \quad (1)$$

Quantification of PCP was performed following the equations described in [Owen *et al.*, 2016] and

[Gussone *et al.*, 2016b]. Equation 2 was used to calculate the present-day site-specific water-calcite fractionation factor using the $\delta^{44}\text{Ca}$ value of the modern precipitate (denoted as δ_A) and the $\delta^{44}\text{Ca}$ value of dripwater samples (denoted as δ_B).

$$\alpha = \frac{\delta_A + 1000}{\delta_B + 1000} \quad (2)$$

Equation 3 is used to calculate the fraction of Ca remaining in solution (f) during carbonate precipitation (i.e. calcium depletion), as a measure of PCP [Owen *et al.*, 2016]. Variables used here are the $\delta^{44}\text{Ca}$ value of the calcitic stalagmite (r_s), the initial dripwater $\delta^{44}\text{Ca}$ value (r_0) before any carbonate precipitation (assumed to be the same as the host rock value), and the $\delta^{44}\text{Ca}$ fractionation factor ($\alpha^{44/40}$) (Eq. 2) between calcite and an aqueous solution [Gussone *et al.*, 2016b].

$$f = \left(\frac{r_s}{\alpha r_0} \right)^{\frac{1}{\alpha-1}} \quad (3)$$

3 Results

3.1 Mineralogy and U-Th chronology

XRD analyses revealed that stalagmite MAW-3_7 and the drip logger sample (MAW-logger) are calcitic, while the second modern carbonate precipitate (MAW-Mod-1) is aragonitic. MAW-3_7 grew from 135 to 99 kyrs BP, covering T II, MIS-5e and the interval encompassing the Late Eemian Arid Period (LEAP, [Sirocko *et al.*, 2005]; Fig. 1b). The chronology is well constrained due to high U concentrations, averaging 4 ppm, resulting in 2σ errors between ± 729 and ± 1432 years (Table S2 in SI). Relatively low growth rates characterized the penultimate glacial ($4 \mu\text{m/yr}$) and the LEAP ($8 \mu\text{m/yr}$) while ten times higher growth rates were observed during MIS-5e ($50 \mu\text{m/yr}$). Although 13 samples were drilled from the stalagmite, only 10 were included in the final age model. Two samples were rejected because their ages (~ 50 kyrs BP) confirmed the presence of a growth hiatus and thus were out of the scope of this study. One sample was excluded because very high Th contents resulted in a large age error (8.4 kyrs).

3.2 Stable isotopes and elemental ratios

MAW-3_7 $\delta^{18}\text{O}$ ranged from -3.43‰ to 0.91‰ VPDB (Fig. 2a). The highest values coincided with T II and the LEAP and lowest values occurred during MIS-5e. Ba/Ca ratios ranged from 0.004 to 0.038 mmol/mol, Sr/Ca ratios from 0.07 to 0.13 mmol/mol and Mg/Ca ratios from 12 to 21 mmol/mol, (Fig. 2b-d). For all elemental ratios, lowest values characterize MIS-5e, while higher values characterize T II and the LEAP. All X/Ca values correlate with each other (Mg/Ca vs. Ba/Ca; $R^2 = 0.27$, $p = 0.07$; Sr/Ca vs. Ba/Ca; $R^2 = 0.28$, $p = 0.07$; Mg/Ca vs. Sr/Ca; $R^2 = 0.87$, $p < 0.0001$) (Fig. S5 in SI). The Ba/Ca record appears almost constant, except for one value, which is one magnitude higher than the rest of the data and skews the correlation with the other elements (without this data point: Mg/Ca vs. Ba/Ca; $R^2 = 0.73$, $p = 0.0004$; Sr/Ca vs. Ba/Ca; $R^2 = 0.87$, $p < 0.00001$). Despite the improved correlation between elemental ratios when excluding this data point, we refrain from treating it as an outlier, as it coincides with the overall maximum in X/Ca in all records. The $\delta^{44}\text{Ca}$ values follow the $\delta^{18}\text{O}$ pattern, ranging from -0.24‰ to -0.88‰ BSE with maxima before and after MIS-5e and lowest $\delta^{44}\text{Ca}$ during MIS-5e (Fig. 2e). We observe a significant positive correlation between $\delta^{18}\text{O}$ and $\delta^{44}\text{Ca}$ ($R^2 = 0.89$, $p = 3.0 \times 10^{-7}$), but no significant correlation between Mg/Ca and $\delta^{44}\text{Ca}$ ($R^2 = 0.5$, $p = 0.15$), Sr/Ca and $\delta^{44}\text{Ca}$ ($R^2 = 0.34$, $p = 0.26$) and Ba/Ca and $\delta^{44}\text{Ca}$ ($R^2 = 0.33$, $p = 0.47$; Fig. S5).

3.3 Reconstructing PCP using Ca isotopes

The modern dripwater $\delta^{44}\text{Ca}$ values (Table S3 in SI) vary depending on the prevailing season. Pre-ISM season dripwater $\delta^{44}\text{Ca}$ varies from -0.01‰ to 0.11‰ (mean = 0.05 ± 0.03 ‰, $n = 5$), while ISM season samples range from 0.00‰ to 0.05‰ (mean = 0.02 ± 0.03 ‰, $n = 2$) and post-ISM waters showed values between 0.02‰ to 0.21‰ (mean = 0.12 ± 0.03 ‰, $n = 2$). MAW-Mod-1 yielded a $\delta^{44}\text{Ca}$ of -1.31‰ ($n=1$), and MAW-logger a $\delta^{44}\text{Ca}$ of -0.66‰ ($n=1$). Coeval measurements of dripwater and glass plate precipitate samples allows for the calculation of the site-specific fractionation factor. We chose the calcitic sample MAW-logger, because MAW-3_7 is also calcitic, and the mean value of all dripwater samples (0.04 ± 0.03 ‰, $n=9$) for our calculations because

MAW-logger itself covers several months of precipitation. A site-specific fractionation of $\alpha^{44/40}=0.99929 \pm 0.00001$ ($\alpha^{44/40}=0.99865 \pm 0.00001$ for the aragonitic sample MAW-Mod-1) was calculated using Equation 1, similar to the effective fractionation factor calculated by Owen et al. (2016) for Heshang Cave ($\alpha=0.99937 \pm 0.00003$). Stalagmite $\delta^{44}\text{Ca}$ ranged from -0.88‰ to 0.24‰ (Fig. 2e). Using the stalagmite $\delta^{44}\text{Ca}$, the site-specific fractionation factor α , and the host rock $\delta^{44}\text{Ca}$ value (mean: -0.15‰ BSE, $n = 2$; Table S3 in SI), which we use to estimate the initial $\delta^{44}\text{Ca}$ of the dripwater prior to any calcite precipitation, in Equation 2 yielded Ca-depletion values (f -values) between 1.00 and 0.42 (i.e., between 0% and 58% Ca-depletion, Fig. 2e).

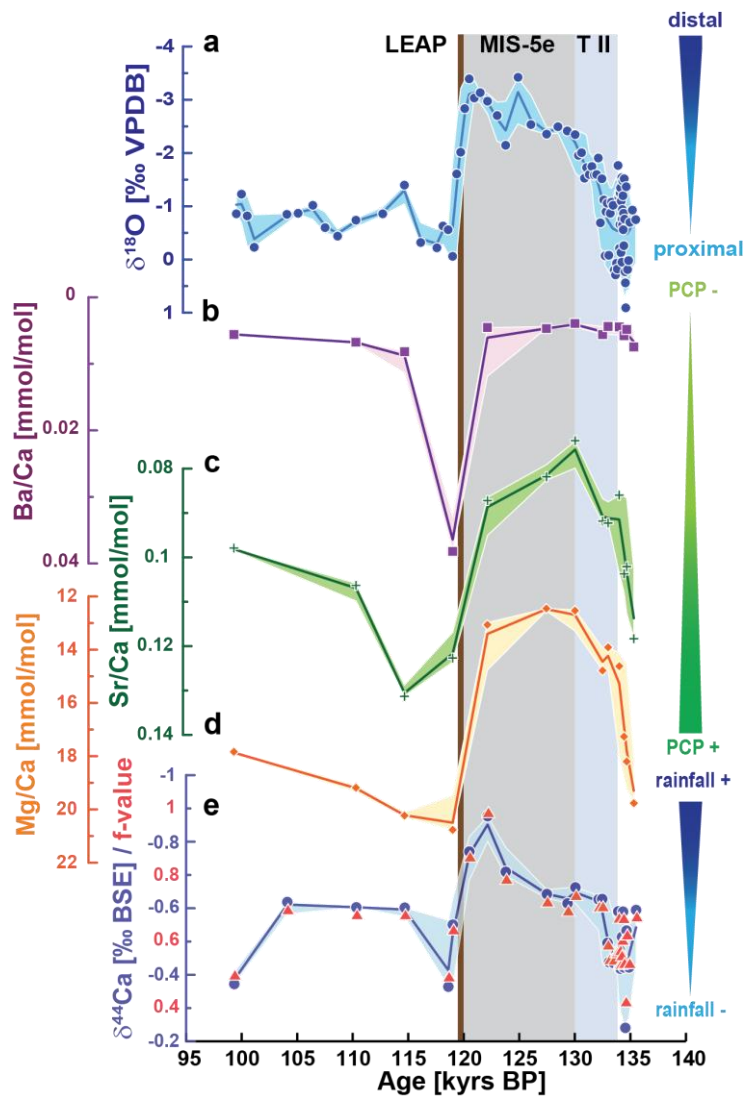


Figure 2: Proxy time series from MAW-3_7: $\delta^{18}\text{O}$ (a); Ba/Ca (b); Sr/Ca (c); Mg/Ca (d); $\delta^{44}\text{Ca}$ and f -value (e); blue vertical shading marks T II, the MIS-5e is marked in grey, and the LEAP as brown line.

4. Discussion

The interpretation of speleothem $\delta^{18}\text{O}$ requires detailed understanding of atmospheric circulation and local climate conditions, such as temperature and precipitation seasonality, rainfall transport pathway, effective infiltration, and vegetation cover [McDermott, 2004; Lachniet, 2009; Breitenbach *et al.*, 2010; Breitenbach *et al.*, 2015; Baker *et al.*, 2015]. This multitude of influencing factors severely hampers quantitative reconstruction of absolute rainfall changes. Using $\delta^{18}\text{O}$, X/Ca, and $\delta^{44}\text{Ca}$ in tandem with modern monitoring data allows us to disentangle local and regional precipitation dynamics using a semi-quantitative approach.

4.1 Oxygen isotopes as tracers of moisture source

At Mawmluh Cave, variations in precipitation $\delta^{18}\text{O}$ reflect a mixed signal of moisture source and rainfall amount [Breitenbach *et al.*, 2010; Breitenbach *et al.*, 2015; Baker *et al.*, 2015]. During the pre- and post-monsoon seasons, the dominant air mass trajectories stem from the proximal BoB, delivering rainwater with relatively high $\delta^{18}\text{O}$ values. With the onset of the ISM, the moisture source shifts to the open Indian Ocean and the Arabian Sea, and the longer transport path lowers the $\delta^{18}\text{O}$ of ISM rainfall. Based on our current understanding, local rainfall $\delta^{18}\text{O}$ generally reflects moisture source variability across the Indian Ocean, and, in broad terms, regional moisture dynamics [Baker *et al.*, 2015].

The *length* of the monsoon season also likely impacts speleothem $\delta^{18}\text{O}$. During the ISM, surface air relative humidity approaches 100%, minimizing re-evaporation of raindrops during their fall through the below-cloud atmosphere. Hence, dripwater reaching the cave would have $\delta^{18}\text{O}$ values close to original unaltered rainfall, yielding more negative speleothem $\delta^{18}\text{O}$ values during periods with, on average, longer wet seasons. This has been previously recognized in speleothem $\delta^{18}\text{O}$ records from northern India and China [Cheng *et al.*, 2009; Orland *et al.*, 2015; Kathayat *et al.*, 2016]. Although mixing of infiltration waters above Mawmluh Cave results in some buffering, a very short (<1 month) isotope signal transfer time (lag) from rain to drip means that such changes in wet season length should be detectable in speleothems at this location [Breitenbach *et al.*, 2015]. However, because of the multiple processes affecting $\delta^{18}\text{O}$, this proxy

alone can not be used to disentangle whether the amount of ISM rainfall, or its seasonal distribution changed. Instead, a combination of $\delta^{18}\text{O}$ and PCP proxies, should allow us to detect changes in seasonality [Ronay *et al.*, 2019]. With ISM rainfall in the range of thousands of mm per ISM season, only an extreme reduction in precipitation amount would induce PCP during the ISM. It is more likely that our PCP proxies (X/Ca and $\delta^{44}\text{Ca}$) indicate changes in the dryness and length of the dry season.

4.2 Trace element ratios as PCP recorders

X/Ca ratios are useful tracers of changes in seasonal water availability. In Mawmluh Cave, trace element incorporation in speleothems is governed by PCP, which is recognized to occur mainly during the dry and pre-ISM seasons [Ronay *et al.*, 2019]. PCP is minimized during the ISM (and post-ISM) when the cave floods and the karst zone is waterlogged. Thus, it is dry and pre-ISM season infiltration which acts as the governing parameter for PCP, informing us on dry season length and reversely ISM duration.

X/Ca ratios are therefore valuable tracers of past *dry season dryness*. Under locally drier conditions, PCP-sensitive Mg/Ca, Sr/Ca and Ba/Ca ratios in MAW-3_7 increase, while they decrease under wetter conditions (Fig. 2). X/Ca increases can be induced by either a shortened ISM (and thus increased rainfall seasonality) or a reduction in dry season rainfall amount (increased dry season dryness), or a combination of both.

Additionally, ventilation-related changes in cave air pCO_2 can influence PCP occurring in the cave and/or epikarst. Stronger ventilation (lower pCO_2) leads to increased PCP, and weaker ventilation (higher pCO_2) to decreased PCP [Ronay *et al.*, 2019]. While the direction of seasonal ventilation changes is corroborated by dry/monsoon season changes, separating the signal of PCP induced by infiltration or by changes in cave air pCO_2 remains challenging. However, Mawmluh Cave experiences only minor seasonal variations in pCO_2 levels, and thus the effect of pCO_2 on PCP is likely minimal, especially when compared to much larger amplitude changes in infiltration. Consequently,

we propose rainfall amount as the major controlling factor on PCP.

4.3 Calcium depletion as infiltration and PCP recorder

Under the assumption of linear scaling of PCP versus rainfall change, a quantitative PCP reconstruction would also allow the quantification of past rainfall amount. Ideally, Ca isotopes should be calibrated against local moisture balance, but in our case this goal could not be met due to logistical challenges, as the cave floods to the ceiling in the wet season. Hence, our interpretation of $\delta^{44}\text{Ca}$ remains semi-quantitative. Although we cannot reconstruct rainfall *amount* quantitatively we can use $\delta^{44}\text{Ca}$ values for a semi-quantitative reconstruction of PCP dynamics. For this, we use the Ca-depletion values (f -values) (Eq. 3), where low $\delta^{44}\text{Ca}$ yield high f -values, and vice versa (Fig. 2e). During PCP, lighter isotopes leave the percolating water preferentially, leading to higher $\delta^{44}\text{Ca}$ values in the remaining solution. In times of high infiltration, PCP will be diminished due to high water-pressure heads and low residence times, resulting in lower $\delta^{44}\text{Ca}$ and higher f -values. During times of low infiltration, i.e. dry seasons, PCP is enhanced and recorded as high $\delta^{44}\text{Ca}$ and low f -values. This relationship is mirrored in modern dripwater, where $\delta^{44}\text{Ca}$ values are lower during the ISM than during the dry season (Fig. S6).

4.4 ISM dynamics during T II, MIS-5e, and the LEAP

Combining the isotopic and elemental data we can characterize ISM dynamics between 135 and 99 kyrs BP and semi-quantitatively estimate PCP changes (Fig. 2). This allows us to disentangle local conditions at the cave site from regional circulation dynamics.

T II was characterized by higher $\delta^{18}\text{O}$, $\delta^{44}\text{Ca}$, and X/Ca values, reflecting a more proximal moisture source, enhanced dry season PCP, and possibly a longer dry season. Increased PCP due to an enhanced/prolonged dry season is also reflected in the very low f -values ($f = 0.42$ to 0.68), which translate to a reduction in dry season precipitation of 10 to 44% relative to modern conditions (Fig. S7), if linear correlation between $\delta^{18}\text{O}$ and $\delta^{44}\text{Ca}$ is assumed [Owen *et al.*, 2016]. As discussed above, this assumption remains untested and the calculated precipitation amounts will need to be carefully evaluated in future studies. Our results are in line with earlier findings of a weaker ISM during T II [Cheng *et al.*, 2009; Kathayat *et al.*, 2016]

During MIS-5e (132 – 116 kyrs BP), lower $\delta^{18}\text{O}$ values relative to T II suggest a strong ISM with a distal moisture source and possibly increased summer rainfall and an overall longer wet season. Lower $\delta^{44}\text{Ca}$ and X/Ca ratios suggest minimal PCP during the dry season, likely suppressed by increased dry season (post-ISM and pre-ISM) rainfall (Fig. 3). From T II until the end of MIS-5e, f -values rise continuously, ranging from 0.70 to 1.0, suggesting an overall increase in dry season precipitation between T II and MIS-5e of up to 60% and an increase of up to 25% relative to modern conditions (Figs. 2; S7).

With the onset of the LEAP, $\delta^{18}\text{O}$, $\delta^{44}\text{Ca}$, and X/Ca ratios increase, suggesting a weakening ISM, with weakened circulation and decreased rainfall amount ($\delta^{18}\text{O}$), a prolonged dry season, and enhanced PCP ($\delta^{44}\text{Ca}$ and X/Ca). Up to 50% reductions in dry season precipitation relative to MIS-5e are observed.

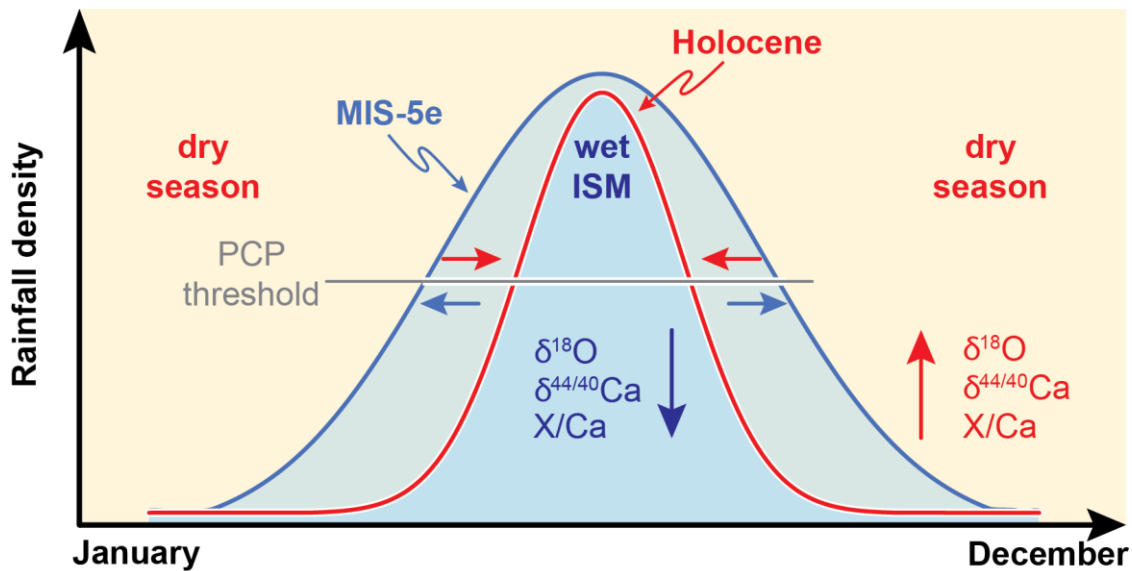


Figure 3: Conceptual model of the meteorological year with rainfall events increasing during the ISM and decreasing during the dry season. Hypothesized rainfall distributions are denoted red for the Holocene and blue for MIS-5e. The grey line denotes the PCP threshold below which PCP is expected and thus the transition from dry season to monsoon season. We assume that MIS-5e was characterized by increased dry season rainfall and increased summer rainfall with abundant extreme events compared to the Holocene. During the dry season, rainfall $\delta^{18}\text{O}$ and PCP increase (higher $\delta^{44}\text{Ca}$ and X/Ca). During the ISM the amount effect is almost negligible, while Rayleigh fractionation leads to lower $\delta^{18}\text{O}$ values and increased infiltration minimized PCP ($\delta^{44}\text{Ca}$ and X/Ca decrease).

In comparison with Holocene stalagmite $\delta^{18}\text{O}$ values from Mawmluh Cave [Berkelhammer *et al.*, 2012; Dutt *et al.*, 2015; Lechleitner *et al.*, 2017], the values in MAW-3_7 during MIS-5e are ca. 4‰ higher. Moreover, $\delta^{44}\text{Ca}$ values during MIS-5e are lower than in the modern precipitates (i.e., our reference point).

This seems counterintuitive, as the warmer MIS-5e should result in a stronger ISM [Fischer *et al.*, 2018] with lower $\delta^{18}\text{O}$ values than during the Holocene. At the same time, lower $\delta^{44}\text{Ca}$ values support the idea of a stronger ISM during MIS-5e with a wetter dry season leading to a reduction in PCP. Unless these offsets are caused by changes in flow paths and mixing history, it is likely MIS-5e was characterized by a change in seasonality with increased dry season infiltration and decreased PCP compared to present times (Fig. 3).

Increased dry season rainfall would be prone to enhanced re-evaporation of early (pre-ISM) and late (post-ISM) rainfall at the cave site, resulting in higher rainfall $\delta^{18}\text{O}$ throughout MIS-5e. At the same time, increased dry season rainfall would minimize PCP, and lead to decreased X/Ca and $\delta^{44}\text{Ca}$ values relative to the Holocene. Thus, our record suggests very strong PCP during T II and the LEAP, reduced PCP during MIS-5e, and some PCP occurring during the Holocene. Additional X/Ca and $\delta^{44}\text{Ca}$ data covering the Holocene are needed to test this hypothesis.

If our proposed scenario is correct, a warmer atmosphere in near future would lead to an intensified ISM season and a wetter dry season (possibly with more extreme events like droughts and floods [Malik *et al.*, 2016]).

5 Conclusions

A high-resolution stalagmite multi-proxy ISM record documents, for the first time, regional and local dynamics of T II and last interglacial rainfall in north-eastern India. The combination of $\delta^{18}\text{O}$, $\delta^{44}\text{Ca}$, and X/Ca ratios unequivocally suggests that during T II and the LEAP conditions were drier than during MIS-5e. Furthermore, in comparison to the Holocene, MIS-5e was likely characterized by a different seasonal distribution of precipitation. We propose that overall the ISM season and the dry season were characterized by higher-than-modern rainfall. This scenario would explain the apparent incongruency between higher-than-modern stalagmite $\delta^{18}\text{O}$ (regional signal), and the simultaneously reduced prior carbonate precipitation in the karst zone (local signal) during MIS-5e.

Coupling $\delta^{44}\text{Ca}$ with X/Ca ratios provides a well-reasoned, semi-quantitative approximation of past rainfall amount. While the accuracy of our tentative reconstruction remains to be validated in future research, it enables the local precipitation signal to be extracted from the regional pattern and represents a significant step towards quantification of past rainfall changes, especially in regions with strong rainfall seasonality.

Acknowledgements

This study received funding from the European Union's Horizon 2020 Research and Innovation programme under the Marie Skłodowska-Curie grant agreement No 691037 (to SFMB, OK, AH). Calcium isotope analyses were supported through ERC StG 307582 CARBONSINK (to AVT), and NERC NE/R013519/1 (to HJB). Financial support came from the National Natural Science Foundation of China (NSFC-41731174, to HC and LE), an award from the palaeoclimate program by the National Science Foundation (NSF-1702816, to HC and LE) and a Rutherford Discovery Fellowship award (RDF-UOW1601, to AH). Gregory Diengdoh (Shillong) is thanked for help during sampling and Ingrid Lindeman (University of Waikato) for assistance in measuring trace elements. We thank Beate Gehnen for assisting with stable isotope analysis. We thank Daniel E. Ibarra and an anonymous reviewer for their critical feedback on earlier versions of this manuscript, and the editorial team of GRL for handling our submission. All data will be archived on www.ncdc.noaa.gov.

References

- Baker, A. J., H. Sodemann, J. U. L. Baldini, S. F. M. Breitenbach, K. R. Johnson, J. van Hunen, and P. Zhang (2015), Seasonality of westerly moisture transport in the East Asian summer monsoon and its implications for interpreting precipitation $\delta^{18}\text{O}$, *J. Geophys. Res. Atmos.*, 120(12), 5850–5862, doi:10.1002/2014JD022919.
- Berger, A., M. Crucifix, D. A. Hodell, C. Mangili, J. F. McManus, B. Otto-Bliesner, K. Pol, Raynaud, D., L. C. Skinner, P. C. Tzedakis, E. W. Wolff, Q. Z. Yin, A. Abe-Ouchi, C. Barbante, V. Brovkin, I. Cacho, E. Capron, P. Ferretti, A. Ganopolski, J. O. Grimalt, B. Hönlisch, K. Kawamura, A. Landais, V. Margari, B. Martrat, V. Masson-Delmotte, Z. Mokeddem, F. Parrenin, A. A. Prokopenko, H. Rashid, M. Schulz, and N. Vazquez Riveiros (2016), Interglacials of the last 800,000 years, *Rev. Geophys.*, 54(1), 162–219, doi:10.1002/2015RG000482.
- Berkelhammer, M., A. Sinha, M. Mudelsee, H. Cheng, R. L. Edwards, and K. Cannariato (2010), Persistent multidecadal power of the Indian Summer Monsoon, *Earth and Planetary Science Letters*, 290(1-2), 166–172, doi:10.1016/j.epsl.2009.12.017.
- Berkelhammer, M., A. Sinha, L. Stott, H. Cheng, F.S.R. Pausata, and K. Yoshimura (2012), An Abrupt Shift in the Indian Monsoon 4000 Years Ago, in *Climates, landscapes, and civilizations, Geophysical Monograph Series*, vol. 198, edited by L. Giosan, pp. 75–88, American Geophysical Union, Washington, D.C.

- Bradbury, H. J., and A. V. Turchyn (2018), Calcium isotope fractionation in sedimentary pore fluids from ODP Leg 175: Resolving carbonate recrystallization, *Geochimica et Cosmochimica Acta*, 236, 121–139, doi:10.1016/j.gca.2018.01.040.
- Breitenbach, S. F. M., and S. M. Bernasconi (2011), Carbon and oxygen isotope analysis of small carbonate samples (20 to 100 μ g) with a GasBench II preparation device, *Rapid communications in mass spectrometry : RCM*, 25(13), 1910–1914, doi:10.1002/rcm.5052.
- Breitenbach, S. F. M., K. Rehfeld, B. Goswami, J. U. L. Baldini, H. E. Ridley, D. J. Kennett, K. M. Prufer, V. V. Aquino, Y. Asmerom, V. J. Polyak, H. Cheng, J. Kurths, and N. Marwan (2012), Constructing Proxy Records from Age models (COPRA), *Clim. Past*, 8(5), 1765–1779, doi:10.5194/cp-8-1765-2012.
- Breitenbach, S. F.M., J. F. Adkins, H. Meyer, N. Marwan, K. K. Kumar, and G. H. Haug (2010), Strong influence of water vapor source dynamics on stable isotopes in precipitation observed in Southern Meghalaya, NE India, *Earth and Planetary Science Letters*, 292(1-2), 212–220, doi:10.1016/j.epsl.2010.01.038.
- Breitenbach, S. F.M., F. A. Lechleitner, H. Meyer, G. Diengdoh, D. Matthey, and N. Marwan (2015), Cave ventilation and rainfall signals in dripwater in a monsoonal setting – a monitoring study from NE India, *Chemical Geology*, 402, 111–124, doi:10.1016/j.chemgeo.2015.03.011.
- Buckley, B. M., R. Fletcher, S.-Y. S. Wang, B. Zottoli, and C. Pottier (2014), Monsoon extremes and society over the past millennium on mainland Southeast Asia, *Quaternary Science Reviews*, 95, 1–19, doi:10.1016/j.quascirev.2014.04.022.
- Burns, S. J. (2002), A 780-year annually resolved record of Indian Ocean monsoon precipitation from a speleothem from south Oman, *J. Geophys. Res.*, 107(D20), 518, doi:10.1029/2001JD001281.
- Cai, Y., I. Y. Fung, R. L. Edwards, Z. An, H. Cheng, J.-E. Lee, L. Tan, C.-C. Shen, X. Wang, J. A. Day, W. Zhou, M. J. Kelly, and J. C. H. Chiang (2015), Variability of stalagmite-inferred Indian monsoon precipitation over the past 252,000 y, *Proceedings of the National Academy of Sciences of the United States of America*, 112(10), 2954–2959, doi:10.1073/pnas.1424035112.
- Cheng, H., R. L. Edwards, W. S. Broecker, G. H. Denton, X. Kong, Y. Wang, R. Zhang, and X. Wang (2009), Ice age terminations, *Science (New York, N.Y.)*, 326(5950), 248–252, doi:10.1126/science.1177840.
- Cheng, H., R. L. Edwards, A. Sinha, C. Spötl, L. Yi, S. Chen, M. Kelly, G. Kathayat, X. Wang, X. Li, X. Kong, Y. Wang, Y. Ning, and H. Zhang (2016), The Asian monsoon over the past 640,000 years and ice age terminations, *Nature*, 534(7609), 640–646, doi:10.1038/nature18591.
- Cheng, H., R. Lawrence Edwards, C.-C. Shen, V. J. Polyak, Y. Asmerom, J. Woodhead, J. Hellstrom, Y. Wang, X. Kong, C. Spötl, X. Wang, and E. Calvin Alexander (2013), Improvements in ^{230}Th dating, ^{230}Th and ^{234}U half-life values, and U–Th isotopic measurements by multi-collector inductively coupled plasma mass spectrometry, *Earth and Planetary Science Letters*, 371–372, 82–91, doi:10.1016/j.epsl.2013.04.006.
- Day, C. C., and G. M. Henderson (2013), Controls on trace-element partitioning in cave-analogue calcite, *Geochimica et Cosmochimica Acta*, 120, 612–627, doi:10.1016/j.gca.2013.05.044.
- Dutt, S., A. K. Gupta, S. C. Clemens, H. Cheng, R. K. Singh, G. Kathayat, and R. L. Edwards (2015), Abrupt changes in Indian summer monsoon strength during 33,800 to 5500 years B.P, *Geophysical research letters*, 42(13), 5526–5532, doi:10.1002/2015GL064015.
- Dykoski, C. A., R. L. Edwards, H. Cheng, D. Yuan, Y. Cai, M. Zhang, Y. Lin, J. Qing, Z. An, and J. Revenaugh (2005), A high-resolution, absolute-dated Holocene and deglacial Asian monsoon record from Dongge Cave, China, *Earth and Planetary Science Letters*, 233(1-2), 71–86, doi:10.1016/j.epsl.2005.01.036.
- Edwards, R. L., J. H. Chen, and G. J. Wasserburg (1987), ^{238}U ^{234}U ^{230}Th ^{232}Th systematics and the precise measurement of time over the past 500,000 years, *Earth and Planetary Science Letters*, 81(2-3), 175–192, doi:10.1016/0012-821X(87)90154-3.
- Fairchild, I. J., and A. Baker (2012), *Speleothem Science*, John Wiley & Sons, Ltd, Chichester, UK.

- Fischer, H., K. J. Meissner, A. C. Mix, N. J. Abram, J. Austermann, V. Brovkin, E. Capron, D. Colombaroli, A.-L. Daniau, K. A. Dyez, T. Felis, S. A. Finkelstein, S. L. Jaccard, E. L. McClymont, A. Rovere, J. Sutter, E. W. Wolff, S. Affolter, P. Bakker, J. A. Ballesteros-Cánovas, C. Barbante, T. Caley, A. E. Carlson, O. Churakova, G. Cortese, B. F. Cumming, B. A. S. Davis, A. de Vernal, J. Emile-Geay, S. C. Fritz, P. Gierz, J. Gottschalk, M. D. Holloway, F. Joos, M. Kucera, M.-F. Loutre, D. J. Lunt, K. Marcisz, J. R. Marlon, P. Martinez, V. Masson-Delmotte, C. Nehrbass-Ahles, B. L. Otto-Bliesner, C. C. Raible, B. Risebrobakken, M. F. Sánchez Goñi, J. S. Arrigo, M. Sarnthein, J. Sjolte, T. F. Stocker, P. A. Velasquez Álvarez, W. Tinner, P. J. Valdes, H. Vogel, H. Wanner, Q. Yan, Z. Yu, M. Ziegler, and L. Zhou (2018), Palaeoclimate constraints on the impact of 2 °C anthropogenic warming and beyond, *Nature Geosci*, 11(7), 474–485, doi:10.1038/s41561-018-0146-0.
- Gussone, N., H. L. Filipsson, and H. Kuhnert (2016a), Mg/Ca, Sr/Ca and Ca isotope ratios in benthonic foraminifers related to test structure, mineralogy and environmental controls, *Geochimica et Cosmochimica Acta*, 173, 142–159, doi:10.1016/j.gca.2015.10.018.
- Gussone, N., A.-D. Schmitt, A. Heuser, F. Wombacher, M. Dietzel, E. Tipper, and M. Schiller (2016b), *Calcium Stable Isotope Geochemistry*, 269 pp., *Advances in Isotope Geochemistry*, Springer Berlin Heidelberg, Berlin, Heidelberg.
- Harouaka, K., M. Mansor, J. L. Macalady, and M. S. Fantle (2016), Calcium isotopic fractionation in microbially mediated gypsum precipitates, *Geochimica et Cosmochimica Acta*, 184, 114–131, doi:10.1016/j.gca.2016.03.003.
- Hippler, D., R. Witbaard, H. M. van Aken, D. Buhl, and A. Immenhauser (2013), Exploring the calcium isotope signature of *Arctica islandica* as an environmental proxy using laboratory- and field-cultured specimens, *Palaeogeography, Palaeoclimatology, Palaeoecology*, 373, 75–87, doi:10.1016/j.palaeo.2011.11.015.
- Jia, J., D. Xia, Y. Wang, B. Wang, H. Lu, and S. Zhao (2016), East Asian monsoon evolution during the Eemian, as recorded in the western Chinese Loess Plateau, *Quaternary International*, 399, 156–164, doi:10.1016/j.quaint.2015.04.006.
- Johnson, K. R., B. Lynn Ingram, W. D. Sharp, and P. Zhang (2006), East Asian summer monsoon variability during Marine Isotope Stage 5 based on speleothem $\delta^{18}\text{O}$ records from Wanxiang Cave, central China, *Palaeogeography, Palaeoclimatology, Palaeoecology*, 236(1-2), 5–19, doi:10.1016/j.palaeo.2005.11.041.
- Kathayat, G., H. Cheng, A. Sinha, C. Spötl, R. L. Edwards, H. Zhang, X. Li, L. Yi, Y. Ning, Y. Cai, W. L. Lui, and S. F. M. Breitenbach (2016), Indian monsoon variability on millennial-orbital timescales, *Scientific reports*, 6, 24374, doi:10.1038/srep24374.
- Kukla, T., M. J. Winnick, K. Maher, D. E. Ibarra, and C. P. Chamberlain (2019), The Sensitivity of Terrestrial $\delta^{18}\text{O}$ Gradients to Hydroclimate Evolution, *J. Geophys. Res. Atmos.*, 124(2), 563–582, doi:10.1029/2018JD029571.
- Lachniet, M. S. (2009), Climatic and environmental controls on speleothem oxygen-isotope values, *Quaternary Science Reviews*, 28(5-6), 412–432, doi:10.1016/j.quascirev.2008.10.021.
- Lechleitner, F. A., S. F. M. Breitenbach, K. Rehfeld, H. E. Ridley, Y. Asmerom, K. M. Prufer, N. Marwan, B. Goswami, D. J. Kennett, V. V. Aquino, V. Polyak, G. H. Haug, T. I. Eglinton, and J. U. L. Baldini (2017), Tropical rainfall over the last two millennia: evidence for a low-latitude hydrologic seesaw, *Scientific reports*, 7, 45809, doi:10.1038/srep45809.
- Li, X., X. Cui, D. He, J. Liao, and C. Hu (2018), Evaluation of the Heshang Cave stalagmite calcium isotope composition as a paleohydrologic proxy by comparison with the instrumental precipitation record, *Scientific reports*, 8(1), 2615, doi:10.1038/s41598-018-20776-5.
- Malik, N., B. Bookhagen, and P. J. Mucha (2016), Spatiotemporal patterns and trends of Indian monsoonal rainfall extremes, *Geophysical research letters*, 43(4), 1710–1717, doi:10.1002/2016GL067841.
- McDermott, F. (2004), Palaeo-climate reconstruction from stable isotope variations in speleothems: A review, *Quaternary Science Reviews*, 23(7-8), 901–918, doi:10.1016/j.quascirev.2003.06.021.

- McIntire, W. L. (1963), Trace element partition coefficients—a review of theory and applications to geology, *Geochimica et Cosmochimica Acta*, 27(12), 1209–1264, doi:10.1016/0016-7037(63)90049-8.
- Myers, C. G., J. L. Oster, W. D. Sharp, R. Bennartz, N. P. Kelley, A. K. Covey, and S. F.M. Breitenbach (2015), Northeast Indian stalagmite records Pacific decadal climate change: Implications for moisture transport and drought in India, *Geophys. Res. Lett.*, 42(10), 4124–4132, doi:10.1002/2015GL063826.
- Orland, I. J., R. L. Edwards, H. Cheng, R. Kozdon, M. Cross, and J. W. Valley (2015), Direct measurements of deglacial monsoon strength in a Chinese stalagmite, *Geology*, 43(6), 555–558, doi:10.1130/G36612.1.
- Owen, R. A., C. C. Day, C.-Y. Hu, Y.-H. Liu, M. D. Pointing, C. L. Blättler, and G. M. Henderson (2016), Calcium isotopes in caves as a proxy for aridity: Modern calibration and application to the 8.2 kyr event, *Earth and Planetary Science Letters*, 443(443), 129–138, doi:10.1016/j.epsl.2016.03.027.
- Railsback, L. B., P. L. Gibbard, M. J. Head, N. R. G. Voarintsoa, and S. Toucanne (2015), An optimized scheme of lettered marine isotope substages for the last 1.0 million years, and the climatostratigraphic nature of isotope stages and substages, *Quaternary Science Reviews*, 111, 94–106, doi:10.1016/j.quascirev.2015.01.012.
- Reynard, L. M., C. C. Day, and G. M. Henderson (2011), Large fractionation of calcium isotopes during cave-analogue calcium carbonate growth, *Geochimica et Cosmochimica Acta*, 75(13), 3726–3740, doi:10.1016/j.gca.2011.04.010.
- Ronay, E. R., S. F. M. Breitenbach, and J. L. Oster (2019), Sensitivity of speleothem records in the Indian Summer Monsoon region to dry season infiltration, *Scientific reports*, 9(1), 5091, doi:10.1038/s41598-019-41630-2.
- Shackleton, N. J., M. F. Sánchez-Goni, D. Pailler, and Y. Lancelot (2003), Marine Isotope Substage 5e and the Eemian Interglacial, *Global and Planetary Change*, 36(3), 151–155, doi:10.1016/S0921-8181(02)00181-9.
- Sherwin, C. M., and J. U.L. Baldini (2011), Cave air and hydrological controls on prior calcite precipitation and stalagmite growth rates: Implications for palaeoclimate reconstructions using speleothems, *Geochimica et Cosmochimica Acta*, 75(14), 3915–3929, doi:10.1016/j.gca.2011.04.020.
- Shukla, R. P., K. C. Tripathi, A. C. Pandey, and I.M.L. Das (2011), Prediction of Indian summer monsoon rainfall using Niño indices: A neural network approach, *Atmospheric Research*, 102(1-2), 99–109, doi:10.1016/j.atmosres.2011.06.013.
- Siccha, M., E. Biton, and H. Gildor (2015), Red Sea circulation during marine isotope stage 5e, *Paleoceanography*, 30(4), 384–401, doi:10.1002/2013PA002603.
- Sinha, A., G. Kathayat, H. Cheng, S. F. M. Breitenbach, M. Berkelhammer, M. Mudelsee, J. Biswas, and R. L. Edwards (2015), Trends and oscillations in the Indian summer monsoon rainfall over the last two millennia, *Nature communications*, 6, 6309, doi:10.1038/ncomms7309.
- Sirocko, F., K. Seelos, K. Schaber, B. Rein, F. Dreher, M. Diehl, R. Lehne, K. Jäger, M. Krbetschek, and D. Degering (2005), A late Eemian aridity pulse in central Europe during the last glacial inception, *Nature*, 436(7052), 833–836, doi:10.1038/nature03905.
- Steuber, T., and D. Buhl (2006), Calcium-isotope fractionation in selected modern and ancient marine carbonates, *Geochimica et Cosmochimica Acta*, 70(22), 5507–5521, doi:10.1016/j.gca.2006.08.028.
- Tadros, C. V., P. C. Treble, A. Baker, I. Fairchild, S. Hankin, R. Roach, M. Markowska, and J. McDonald (2016), ENSO—cave drip water hydrochemical relationship: a 7-year dataset from south-eastern Australia, *Hydrol. Earth Syst. Sci.*, 20(11), 4625–4640, doi:10.5194/hess-20-4625-2016.
- Wang, Y. J., H. Cheng, R. L. Edwards, Z. S. An, J. Y. Wu, C. C. Shen, and J. A. Dorale (2001), A high-resolution absolute-dated late Pleistocene Monsoon record from Hulu Cave, China, *Science (New York, N.Y.)*, 294(5550), 2345–2348, doi:10.1126/science.1064618.

- Yan, H., A.-D. Schmitt, Z. Liu, S. Gangloff, H. Sun, J. Chen, and F. Chabaux (2016), Calcium isotopic fractionation during travertine deposition under different hydrodynamic conditions: Examples from Baishuitai (Yunnan, SW China), *Chemical Geology*, 426, 60–70, doi:10.1016/j.chemgeo.2016.02.002.
- Yin, Q., and A. Berger (2015), Interglacial analogues of the Holocene and its natural near future, *Quaternary Science Reviews*, 120, 28–46, doi:10.1016/j.quascirev.2015.04.008.
- Yuan, D., H. Cheng, R. L. Edwards, C. A. Dykoski, M. J. Kelly, M. Zhang, J. Qing, Y. Lin, Y. Wang, J. Wu, J. A. Dorale, Z. An, and Y. Cai (2004), Timing, duration, and transitions of the last interglacial Asian monsoon, *Science (New York, N.Y.)*, 304(5670), 575–578, doi:10.1126/science.1091220.
- Ziegler, M., L. J. Lourens, E. Tuenter, F. Hilgen, G.-J. Reichert, and N. Weber (2010), Precession phasing offset between Indian summer monsoon and Arabian Sea productivity linked to changes in Atlantic overturning circulation, *Paleoceanography*, 25(3), 732, doi:10.1029/2009PA001884.

Figure 1.

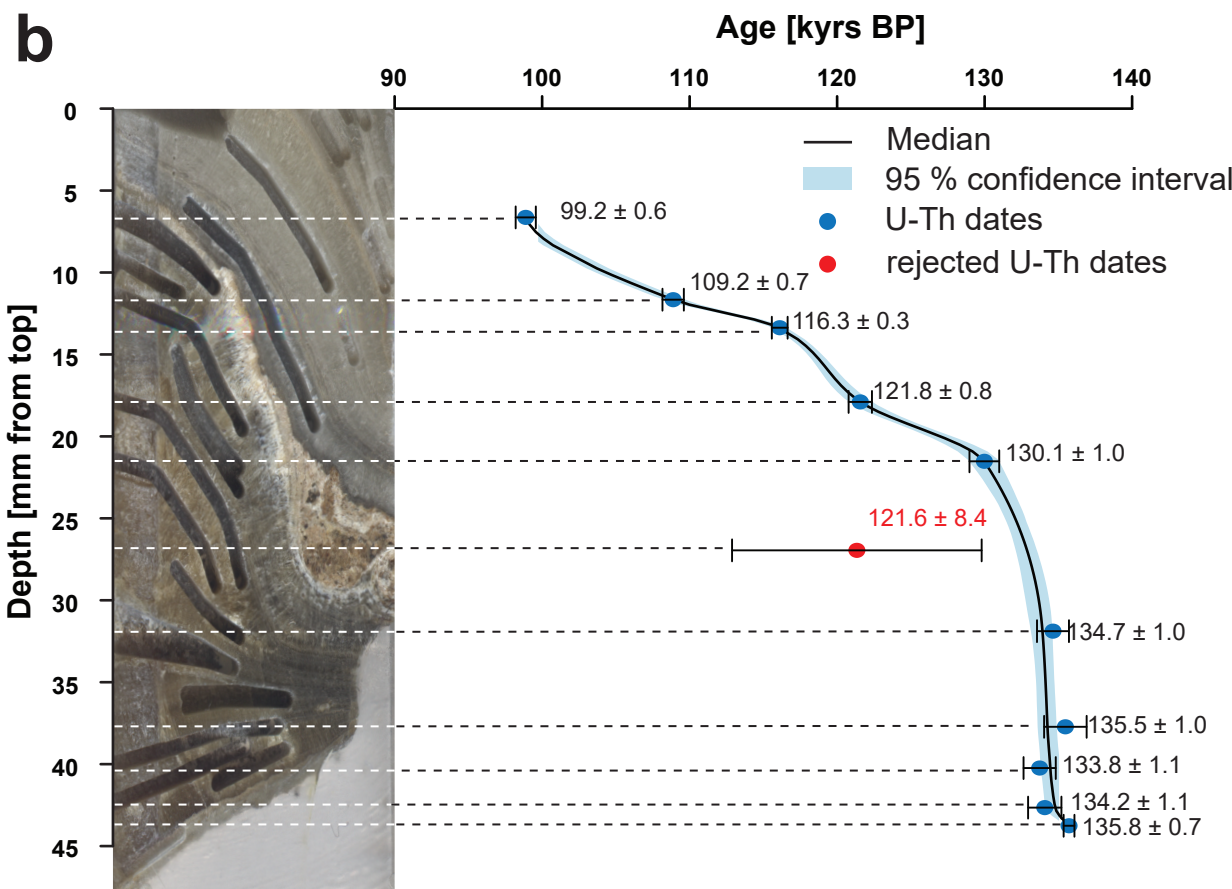
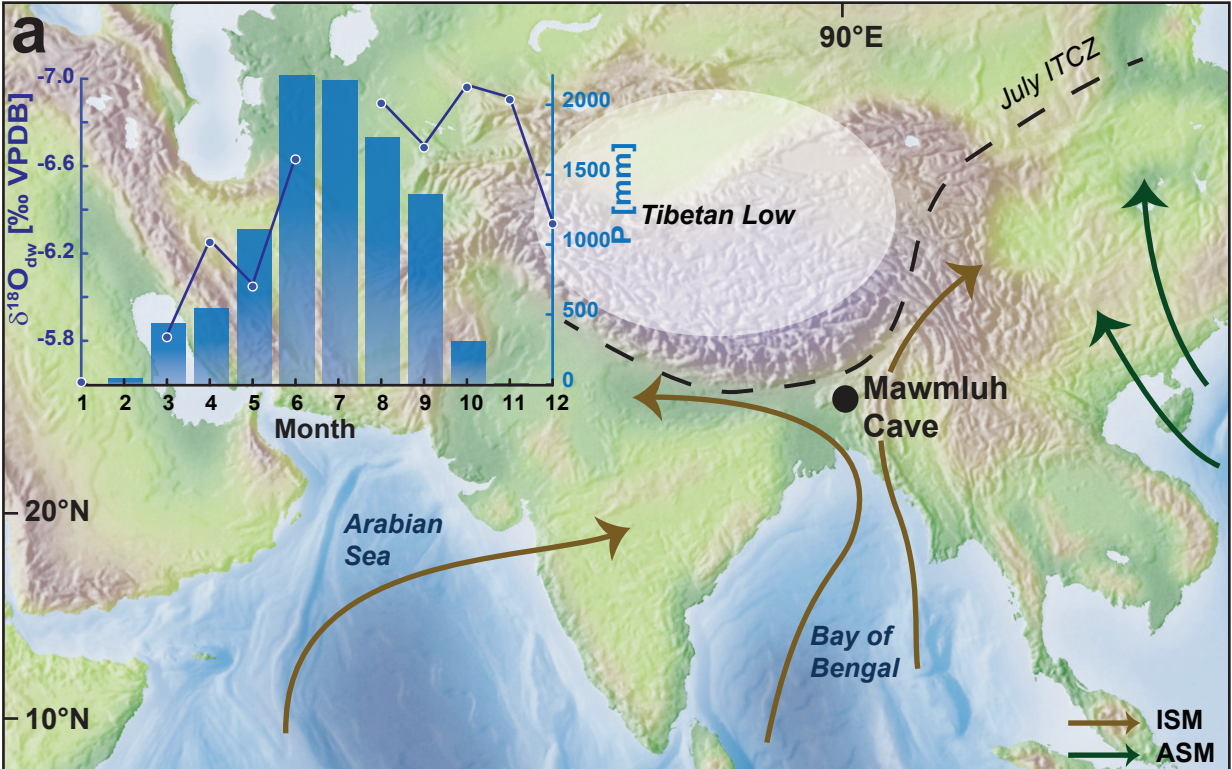


Figure 2.

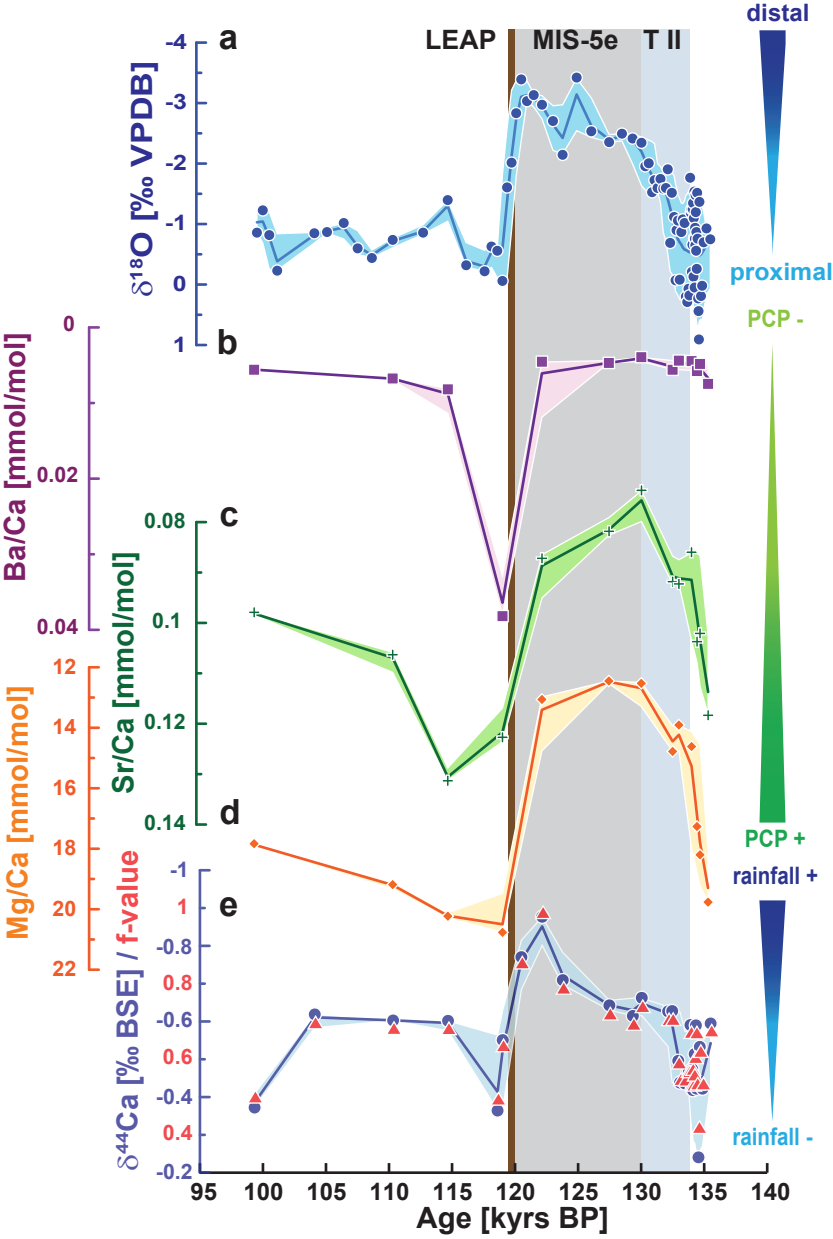


Figure 3.

